Biocompatibility of Ceramic Materials in Ca$_2$P$_2$O$_7$_Ca(PO$_3$)$_2$ System Obtained via Heat Treatment of Cement-Salt Stone

Otabek Toshev [1,*]**, Tatiana Safronova** [1,2]ⓘ**, Maksim Kaimonov** [1]ⓘ**, Tatiana Shatalova** [1,2]**, Elena Klimashina** [2]**, Yulia Lukina** [3]**, Konstantin Malyutin** [4] **and Sergey Sivkov** [5]

[1] Department of Materials Science, Lomonosov Moscow State University, Building, 73, Leninskie Gory, 1, 119991 Moscow, Russia

[2] Department of Chemistry, Lomonosov Moscow State University, Building, 3, Leninskie Gory, 1, 119991 Moscow, Russia

[3] National Medical Research Center for Traumatology and Orthopedics named after N.N. Priorov, Priorova, 10, 127299 Moscow, Russia

[4] Skolkovo Institute of Science and Technology, Bolshoy Boulevard, 30, 121205 Moscow, Russia

[5] Faculty of Technology of Inorganic Substances and High-Temperature Materials, Mendeleev University of Chemical Technology of Russia, Miusskaya pl., 9, 125047 Moscow, Russia

[*] Correspondence: toshevou@my.msu.ru; Tel.: +7-977-522-50-62

Abstract: Biocompatibility of ceramic materials in Ca$_2$P$_2$O$_7$-Ca(PO$_3$)$_2$ system was investigated using different methods, including in vitro and in vivo tests. Ceramic materials in the Ca$_2$P$_2$O$_7$-Ca(PO$_3$)$_2$ system were obtained by annealing cement-salt stone based on powder mixtures of calcium citrate tet-rahydrate Ca$_3$(C$_6$H$_5$O$_7$)$_2$·4H$_2$O and monocalcium phosphate monohydrate (MCPM) Ca(H$_2$PO$_4$)$_2$·H$_2$O. The phase composition of cement-salt stone included brushite, monetite as a result of chemical reaction of starting components after adding of water. The presence of citric acid as by-product of chemical reaction, leads to increase the setting time of the cement-salt stone. Highly concentrated aqueous suspensions based on calcium citrate and MCPM powders providing content of calcium polyphosphate Ca(PO$_3$)$_2$ up to 20 wt % in ceramics were used for designing bioresorbable materials. The presence of an excess of monocalcium phosphate monohydrate makes it possible to reduce the annealing temperature of ceramics, which is associated with the formation of a lower melting phase of Ca(PO$_3$)$_2$. In vivo tests shown that obtained ceramic materials can be recommended for regenerative treatments for bone defects.

Keywords: brushite; monetite; cement-salt stone; calcium pyrophosphate; calcium polyphosphate; ceramics; biocompatibility

1. Introduction

Calcium phosphate ceramic materials are widely used in regenerative medicine for the treatment or replacement of damaged bone tissue due to their excellent biocompatibility [1–3]. Materials, which are used in regenerative medicine, must be resorbable. Despite the great progress in the development of ceramic materials based on calcium phosphates, nowadays increasing resorbability of the biomaterials is one of the main challenges of materials science.

One of the main inorganic components of human bone tissue is hydroxyapatite Ca$_{10}$(PO$_4$)$_6$(OH)$_2$ Ca/P = 1.67, which is a low-rate resorbable material. Synchronization of the rate of material resorption and the rate of the growth of new bone tissue is required to enhance the bone regeneration process.

In this regard, the key characteristic of the material is its ability to resorb in the environment of the body. To increase the resorbability of ceramic materials, the concept of using calcium pyrophosphate Ca$_2$P$_2$O$_7$ and calcium polyphosphates Ca(PO$_3$)$_2$ has been developed. Generally, these materials have a Ca to P ratio of 1 and 0.5 correspondingly,

which are lower than that of hydroxyapatite $Ca_{10}(PO_4)_6(OH)_2$ and possess increased resorbability [4,5]. Therefore, ceramics based on calcium phosphates with a low Ca/P ratio are of huge scientific interest for designing materials for bone implants [6–12].

Ceramics based on $Ca_2P_2O_7$ were obtained by applying direct powder precursors [13]. Direct precursors are calcium phosphate, which have a Ca/P ratio equal to the ratio of the ceramic phase [13]. Such precursors are brushite ($CaHPO_4 \cdot 2H_2O$) [14,15], monetite ($CaHPO_4$) [16,17], γ-$Ca_2P_2O_7$ [18], and β-$Ca_2P_2O_7$ [19]. There are also indirect precursors that are a mixture of calcium phosphates with a ratio of Ca/P = 1. In this case, the formation of the $Ca_2P_2O_7$ phase was observed at the stage of heat treatment of a ceramic material, which was associated with the heterophase reaction between the starting substances and the products of their thermal conversion [20]. Ceramics based on $Ca_2P_2O_7$ are annealed at temperatures below 1150 °C [21,22]. The addition of a lower melting phase of $Ca(PO_3)_2$ can significantly reduce the annealing temperature. Depending on the annealing temperature, various polymorphic modifications of $Ca_2P_2O_7$ can be obtained: amorphous calcium pyrophosphate at 450 °C; γ-$Ca_2P_2O_7$–at 530 °C, β–$Ca_2P_2O_7$ at 700–750 °C, and α–$Ca_2P_2O_7$ at 1140–1179 °C [23].

Calcium polyphosphate can be obtained by polycondensation of the MCPM $Ca(H_2PO_4)_2 \cdot H_2O$:

$$nCa(H_2PO_4)_2 \cdot H_2O \rightarrow (Ca(PO_3)_2)n \qquad (1)$$
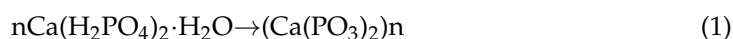
In the temperature range of 690–750 °C, γ–$Ca(PO_3)_2$ transforms into β–$Ca(PO_3)_2$, but at temperatures above 750 °C, the β–modification transforms into the α–modification [24].

Materials in the $Ca_2P_2O_7$-$Ca(PO_3)_2$ system with a reduced firing temperature and up to 40 wt % of calcium polyphosphate have been developed, but their properties such as strength and biocompatibility have not been investigated [5]. These ceramic materials were obtained by annealing cement-salt stone formed from highly concentrated hardening suspensions including calcium citrate tetrahydrate $Ca_3(C_6H_5O_7)_2 \cdot 4H_2O$ and monocalcium phosphate monohydrate $Ca(H_2PO_4)_2 \cdot H_2O$. The phase composition and microstructure of the materials were investigated using X-Ray diffraction analysis and scanning electron microscopy. It was found that the presence of 40 wt % of calcium polyphosphate coused the crucial degradation of ceramics' microstructure due to abnormal grain growth.

Therefore, the purpose of this work consisted in investigation of biocompatibility of ceramics based on calcium pyrophosphate $Ca_2P_2O_7$ and calcium polyphosphate $Ca(PO_3)_2$ with content up to 20 wt. % using in vitro and in vivo tests. The obtained materials were investigated in the simulated body fluid (SBF) and in vivo model mediums.

2. Materials and Methods

2.1. Initial Reagents and Synthesis

Calcium citrate tetrahydrate $Ca_3(C_6H_5O_7)_2 \cdot 4H_2O$ (CAS No. 5785-44-4, puriss. p.a. ≥85%) and monocalcium phosphate monohydrate $Ca(H_2PO_4)_2 \cdot H_2O$ (CAS No. 10031-30-8, puriss. 99%) for the synthesis of ceramic materials were purchased from Sigma Aldrich, (Taufkirchen, Germany).

2.2. Preparation of the Calcium Pyrophosphate and Calcium Polyphosphate Ceramics

A highly concentrated aqueous suspension was obtained by mixing calcium citrate and MCPM powders. These salts were mixed with each other in a such way that calcium pyrophosphate and calcium polyphosphate were present in the final ceramic product in the following ratios: $Ca(PO_3)_2/Ca_2P_2O_7$ = 0/100; 5/95; 10/90; and 20/80 (Table 1). The amount of the used calcium citrate and monocalcium phosphate monohydrate were calculated according to the following reaction:
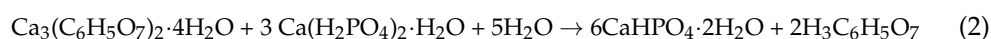
$$Ca_3(C_6H_5O_7)_2 \cdot 4H_2O + 3\,Ca(H_2PO_4)_2 \cdot H_2O + 5H_2O \rightarrow 6CaHPO_4 \cdot 2H_2O + 2H_3C_6H_5O_7 \qquad (2)$$

Table 1. The specified phase composition of the ceramic materials and corresponding composition of the samples after formation.

No	Expected Phase Composition of Ceramics		Expected Phase Composition of Samples after Forming	
	β-Ca(PO$_3$)$_2$ (g)	β-Ca$_2$P$_2$O$_7$ (g)	Ca(H$_2$PO$_4$)$_2$·H$_2$O (g)	CaHPO$_4$·2H$_2$O (g)
1	0	100	0	135.4
2	5	95	6,4	128.7
3	10	90	12,7	121.9
4	20	80	25,4	108.3

A ceramic based on pyrophosphate and calcium polyphosphate was obtained by molding and subsequent annealing of brushite cement stone at a temperature range of 800–1000 °C for 3 h.

2.3. Characterization

The X-ray diffraction (XRD) analysis was conducted using a Rigaku D/Max-2500 (Rigaku, Tokyo, Japan).

The microstructure of the ceramic materials was studied using a LEO SUPRA 50VP (Carl Zeiss, Oberkochen, Germany) scanning electron microscope (SEM) with an acceleration voltage of 21 kV. The images were recorded using Everhart-Thornley secondary electron detector.

2.3.1. Determination of Plastic Strength

The cone penetrometric method [25] was applied to determine the plastic strength of the obtained composites. A Rebinder conical plastometer (CP-3, Moscow, USSR) was used to measure the plastic strength. The plastic strength of the system was calculated by the formula:

$$R = \frac{L}{l} \cdot k \cdot \frac{F}{h^2} \tag{3}$$

where R is the plastic strength [MPa]; L/l is the plastometer shoulders ratio (length in cm); and k is the dimensionless coefficient, which depends on the angular opening of the cone.

$$k = \frac{\cos^2 \frac{\alpha}{2} \operatorname{ctg} \frac{\alpha}{2}}{\pi} \tag{4}$$

where $\alpha = 60°$ and k = 0.413.

2.3.2. Determination of Strength Properties

To determine the strength characteristics, the obtained ceramics, balks with characteristic sizes of $10 \times 10 \times 30$ mm, were formed from cement paste. The water/solid ratio was 0.5 for cements based on calcium citrate and monocalcium phosphate monohydrate. The resulting cement dough was mixed in a Teflon porcelain bowl for 30 s.

The bending and compressive strengths of the samples were determined using universal testing machines LFV 10-T50 and P-05 (Walter + bai, Löhningen Switzerland).

2.3.3. Determination of True Density

Density of the materials/samples was determined via the pycnometric method. The density of the materials was estimated using Equation (5):

$$\rho = \frac{(m_1 - m_2) \cdot \rho(\kappa)}{(m_2 - m_1) + (m_4 - m_3)} \tag{5}$$

where m_1 is the weight of empty pycnometer [g]; m_2 is the weight of pycnometer with powder [g]; m_3 is the weight of pycnometer with powder and liquid [g]; m_4 is the weight of pycnometer with liquid [g]; ρ (κ) is the density of kerosene [g/cm^3].

2.3.4. Thermal Analysis

The thermal analysis (TA) was carried out on a NETZSCH STA 409 PC Luxx thermal analyzer (NETZSCH, Selb, Germany). The heating rate was 10 °C/min and the temperature range was 20–1000 °C. The weight of the samples for the measurements was about 10 mg. The composition of the gas phase formed upon the decomposition of samples was studied using a QMS 403C Aëolos quadrupole mass spectrometer (NETZSCH, Selb, Germany) coupled to a NETZSCH STA 409 PC Luxx thermal analyzer. Mass spectra (MS) were recorded for m/z 18 (H_2O) as well as for m/z 44 (CO_2).

2.3.5. pH Measurements

The study of ion activity in solutions (pH) was carried out using a multichannel ion meter Econix-Expert-001 (Russia) equipped with a glass electrode. Calibration of the electrodes was conducted using solutions with known concentrations of the ions and standard buffer solutions with a given pH.

The pH measurements were performed at room temperature (25 °C) for one day at a powder/water mass ratio of 1/125. The data were recorded every 1 s.

2.3.6. In Vivo Tests

The animal study protocol was approved by the Institutional Review Board (or Ethics Committee) of National Medical Research Center for Traumatology and Orthopedics named after N.N. Priorov, Ministry of Health of the Russian Federation (protocol code 005, date of approval 12.05.2021). The methods used in the work comply with the approved ISO 10993 standards; among them ISO 10993-2-2009 (Animal welfare requirements); ISO 10993-5-2011 (Tests for in vitro cytotoxicity); ISO 10993-6-2021 (Tests for local effects after implantation).

In vivo tests were performed using a model of subcutaneous implantation on Wistar rats. The preclinical assessment of the biocompatibility, resorption, and antibacterial effect of the obtained calcium phosphate matrices were carried out in vivo on five male Wistar rats weighing 250–300 g using a model of ectopic osteogenesis. Histological examination of the morphological changes was studied using standard light microscopy, phase contrast and polarization microscopy in a Leica DM 4000 B LED microscope with a Leica DFC 7000 T camera (Wetzlar, Germany). Thin sections were stained with hematoxylin and eosin. As part of the histological study, a morphometric analysis of the revealed morphological signs was carried out by the method of semi-quantitative scoring. The signs were assessed using a five-point system. The presence of macrophages, fibroblasts, and lymph-macrophage infiltration was assessed on a scale:

4—no sign;
3—weakly expressed sign;
2—moderately pronounced sign;
1—a well-defined sign;
0—the most pronounced sign

Fibrous capsule maturity, thickness, and vascularization on a scale:

0—no sign;
1—weakly expressed sign;
2—moderately pronounced sign;
3—a well-defined sign;
4—the most pronounced sign.

The biocompatibility was assessed by summing the average scores for each trait in each sample in the group.

3. Results and Discussion

Figure 1 represents the dependence of the plastic strength on time for different components of mixtures of calcium citrate and MCPM.
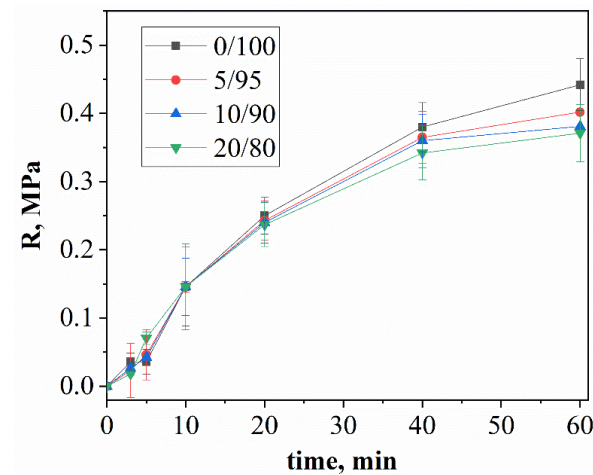

Figure 1. The time dependence of the plastic strength of cement stone with a weight ratio of: $Ca(PO_3)_2/Ca_2P_2O_7 = 0/100$; $Ca(PO_3)_2/Ca_2P_2O_7 = 5/95$; $Ca(PO_3)_2/Ca_2P_2O_7 = 10/90$; $Ca(PO_3)_2/Ca_2P_2O_7 = 20/80$.

The increase in the plastic strength is associated with the process of the hardening of cement solutions and the formation of cement stone. In the first 10 min after mixing the cement pastes, the plastic strength increased faster for compositions containing high volumes of MCPM. The rate of brushite formation at this stage was limited by the rate of the dissolution of calcium citrate, which increased with an excess of acidic MCPM. Furthermore, the change in plastic strength is different for different compositions: the plastic strength was inversely proportional to the concentration of MCPM in the initial mixtures. The plastic strength depends on the rate of the formation of cement stone and the adhesion strength between the newly formed crystals: an increase in the amount of MCPM in the initial mixture led to a decrease in the proportion of brushite with lamellar crystals in the final product, which formed smaller contacts with each other and, accordingly, resulted in a low plastic strength.

Sample, which was shown in Figure 2, is the practical confirmation of the idea of slowing down the setting time allowed for layer-by-layer printing.

Figure 2. Sample after extrusion 3D-printing prepared from highly concentrated hardening suspensions ($Ca(PO_3)_2/Ca_2P_2O_7 = 0/100$).

The XRD patterns of the cement stone based on calcium citrate and MCPM are shown in Figure 3.

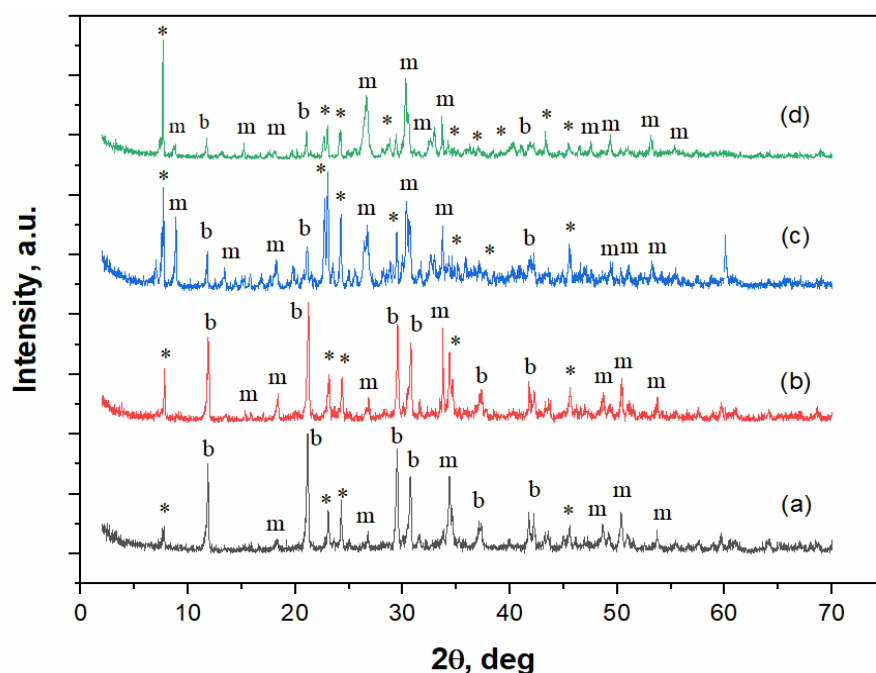**Figure 3.** The XRD spectra of the cement-salt stone obtained from calcium citrate tetrahydrate and MCPM mixture with weight ratio of: (**a**) $Ca(PO_3)_2/Ca_2P_2O_7 = 0/100$; .*–$Ca(H_2PO_4)_2 \cdot H_2O$ (PDF 9-347); b–$CaHPO_4 \cdot 2H_2O$ (PDF 72-713); m–$CaHPO_4$ (PDF 75-1520). (**b**) $Ca(PO_3)_2/Ca_2P_2O_7 = 5/95$, (**c**) $Ca(PO_3)_2/Ca_2P_2O_7 = 10/90$, (**d**) $Ca(PO_3)_2/Ca_2P_2O_7 = 20/80$.

According to the XRD data, the phase composition of cement-salt stone with different ratios of MCPM to calcium citrate (Figure 3) is represented by brushite, monetite, and unreacted MCPM phases. Increasing the MCPM to calcium citrate molar ratio led to an increase in the monetite phase and a decrease in the brushite phase, as determined by the intensity of the corresponding XRD peaks. The increase in the monetite content was associated with its higher thermodynamic stability at lower pH values [26], which was due to an increase in the amount of MCPM in the composition of the cement mixture.

The cement-salt stone formed at a $Ca(PO_3)_2/Ca_2P_2O_7$ ratio of 0/100 had thick rod-like crystals with a small amount of lamellar structure (Figure 4).

An increase in the MCPM content in the initial mixture led to an increase in the content of thin, lamellar crystals of different sizes, which is most likely associated with the conditions of supersaturation and the rapid formation of crystals of the newly formed phases. The cement stone obtained from the initial mixture composition of 20/80 had a bigger crystalline size compared to the other compositions.

The mechanical strength of cement stone was inversely proportional to the concentration of MCPM in the initial cement mixture, which was associated with a decrease in the amount of the final product (brushite) per unit volume with an increase in MCPM (Figure 5). This was due to the presence of lamellar crystals and less cohesion with each other.

The thermal analysis of the obtained samples is shown in Figure 6: the temperature dependence of the mass of formed samples (Figure 6a), the temperature dependence of the ion current for water m/Z = 18 (H_2O) (Figure 6b), and carbon dioxide m/Z = 44 (CO_2) (Figure 6c). We can suggest the following reactions that can take place during heating:
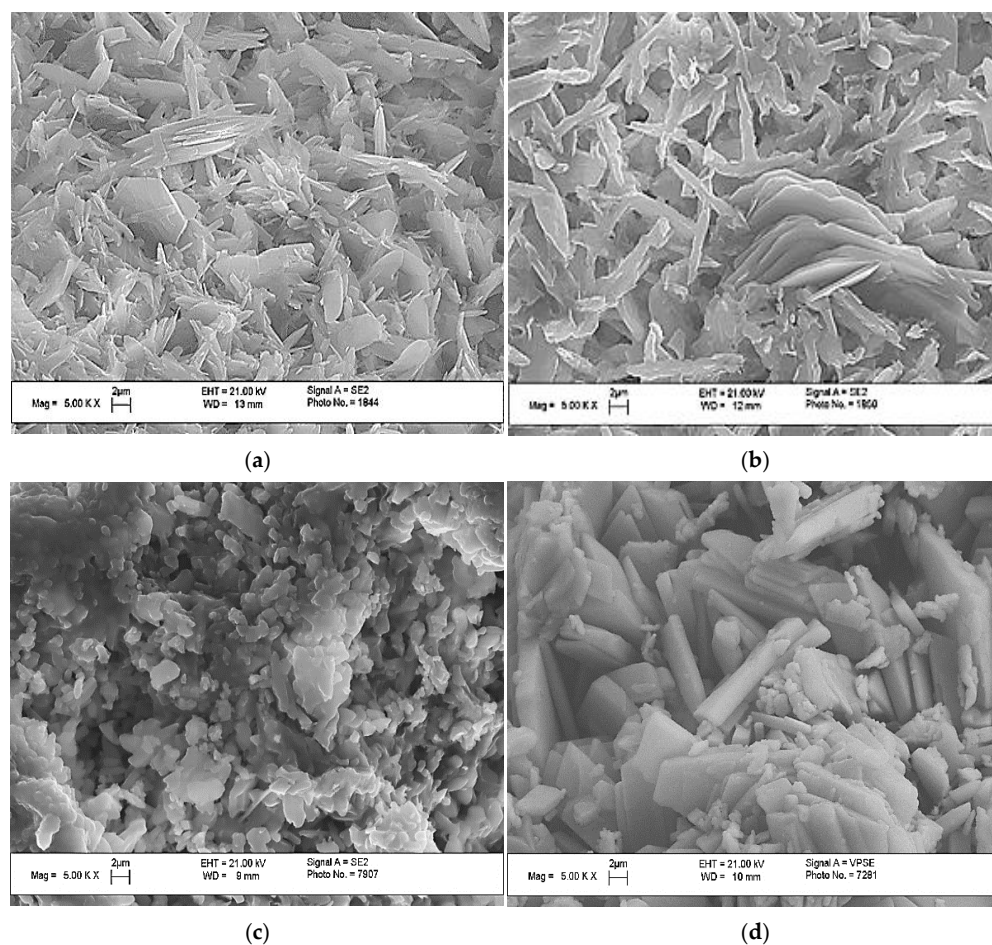
$$CaHPO_4 \cdot 2H_2O \rightarrow CaHPO_4 + 2H_2O \tag{6}$$

$$CaHPO_4 \rightarrow Ca_2P_2O_7 + H_2O \tag{7}$$
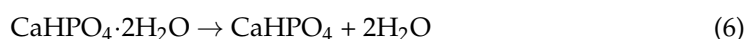
Figure 4. The SEM images of the cement stone, with a weight ratio of: (**a**) $Ca(PO_3)_2/Ca_2P_2O_7 = 0/100$; (**b**) $Ca(PO_3)_2/Ca_2P_2O_7 = 5/95$; (**c**) $Ca(PO_3)_2/Ca_2P_2O_7 = 10/90$; (**d**) $Ca(PO_3)_2/Ca_2P_2O_7 = 20/80$.

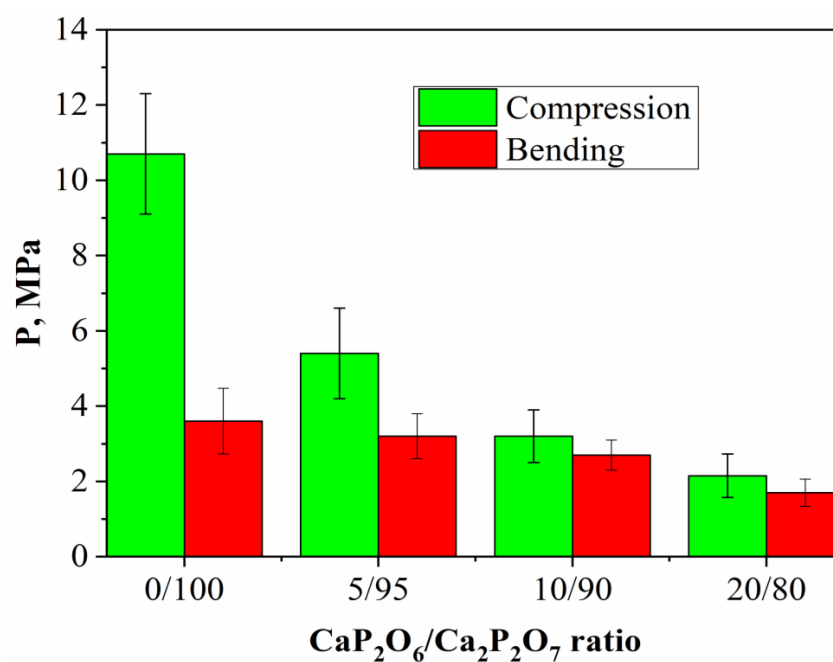**Figure 5.** The compressive and bending strengths of the cement-salt stone with the weight ratio of: $Ca(PO_3)_2/Ca_2P_2O_7 = 0/100$; $Ca(PO_3)_2/Ca_2P_2O_7 = 5/95$; $Ca(PO_3)_2/Ca_2P_2O_7 = 10/90$; $Ca(PO_3)_2/Ca_2P_2O_7 = 20/80$.

The mass loss curve for sample 0/100 contains steps characteristic of brushite, namely, the conversion of brushite to monetite (~200 °C, equation 6), and then monetite to pyrophosphate (~400 °C, equation 7). The presence of unreacted starting components in the samples (a component taken in excess) and the accompanying reaction products determine the presence of additional steps of mass loss and peaks on the curves of the dependence of the ion current on temperature (Figure 6b,c). The curves of the dependences of the ion current for water (MS, m/Z = 18) for samples 0/100, 5/95, 10/90, and 20/80 are shown in Figure 6b. In this graph, peaks of CO_2 can be seen in the range of 160–250 °C, the presence of which can be attributed to the decomposition of the co-product of the reaction of the formation of brushite–citric acid ($t_{decom.}$ = 175 °C). The intensity of this peak increased with the increasing content of MCPM in the composition of the initial mixture. The excess of this initial component apparently contributes to a more complete equation (2), which leads to the formation of a large amount of citric acid.
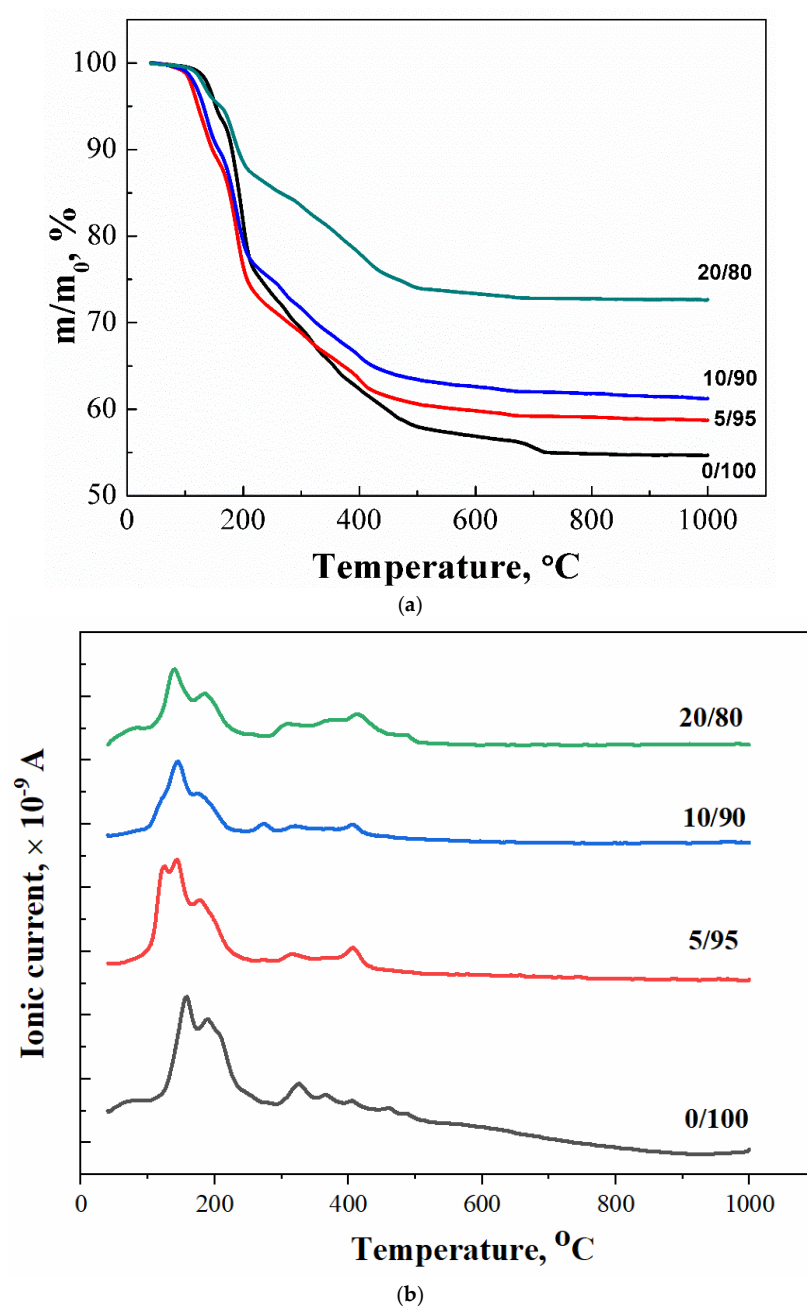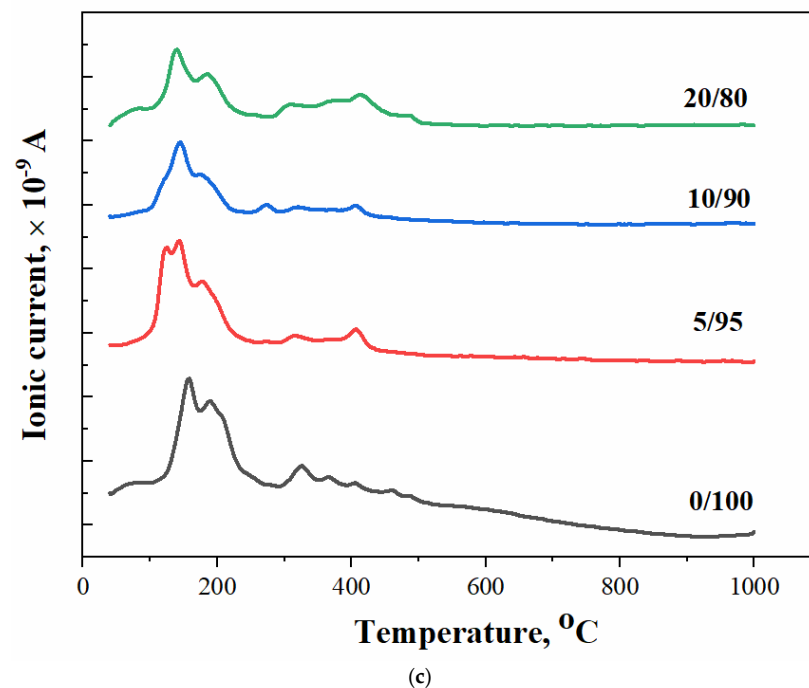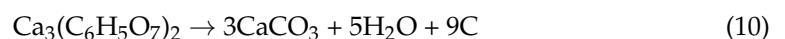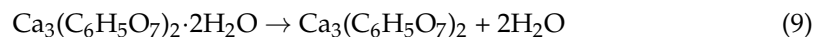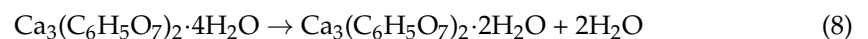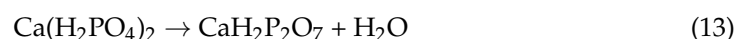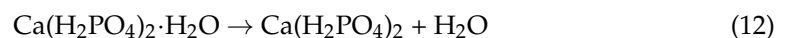

(a)

(b)

Figure 6. *Cont.*

(c)

Figure 6. The thermal analysis of synthesized brushite powders from calcium citrate and MCPM: (**a**) powder mass versus temperature upon heating; (**b**,**c**) ion current curves according to mass spectroscopy for m/Z = 18 (H_2O) (**b**) and for m/Z = 44 (CO_2) (**c**), respectively.

Thermal decomposition of calcium citrate tetrahydrate $Ca_3(C_6H_5O_7)_2 \cdot 4H_2O$ of the samples in the air is sequentially realized by the following reactions [27]:

$$Ca_3(C_6H_5O_7)_2 \cdot 4H_2O \rightarrow Ca_3(C_6H_5O_7)_2 \cdot 2H_2O + 2H_2O \tag{8}$$

$$Ca_3(C_6H_5O_7)_2 \cdot 2H_2O \rightarrow Ca_3(C_6H_5O_7)_2 + 2H_2O \tag{9}$$

$$Ca_3(C_6H_5O_7)_2 \rightarrow 3CaCO_3 + 5H_2O + 9C \tag{10}$$

$$CaCO_3 = CaO + CO_2 \tag{11}$$

MCPM $Ca(H_2PO_4)_2 \cdot H_2O$ present in the samples also undergoes a series of transformations [28], forming calcium polyphosphate $Ca(PO_3)_2$:

$$Ca(H_2PO_4)_2 \cdot H_2O \rightarrow Ca(H_2PO_4)_2 + H_2O \tag{12}$$

$$Ca(H_2PO_4)_2 \rightarrow CaH_2P_2O_7 + H_2O \tag{13}$$

$$CaH_2P_2O_7 \rightarrow Ca(PO_3)_2 + H_2O \tag{14}$$

The phase composition of ceramic materials 0/100 and 20/80, obtained by annealing the cement stone based on $Ca_3(C_6H_5O_7)_2 \cdot 4H_2O$ and $Ca(H_2PO_4)_2 \cdot H_2O$, was consistent with the data of true density (Figure 7a,b), respectively. After annealing at the temperature of 600 °C, a calcium polyphosphate phase was observed in all compositions. When the temperature increased to 1000 °C, calcium polyphosphate transformed to calcium pyrophosphate. This was due to the thermal decomposition of $Ca(PO_3)_2$ at temperatures above 900 °C to calcium pyrophosphate according to the equation:
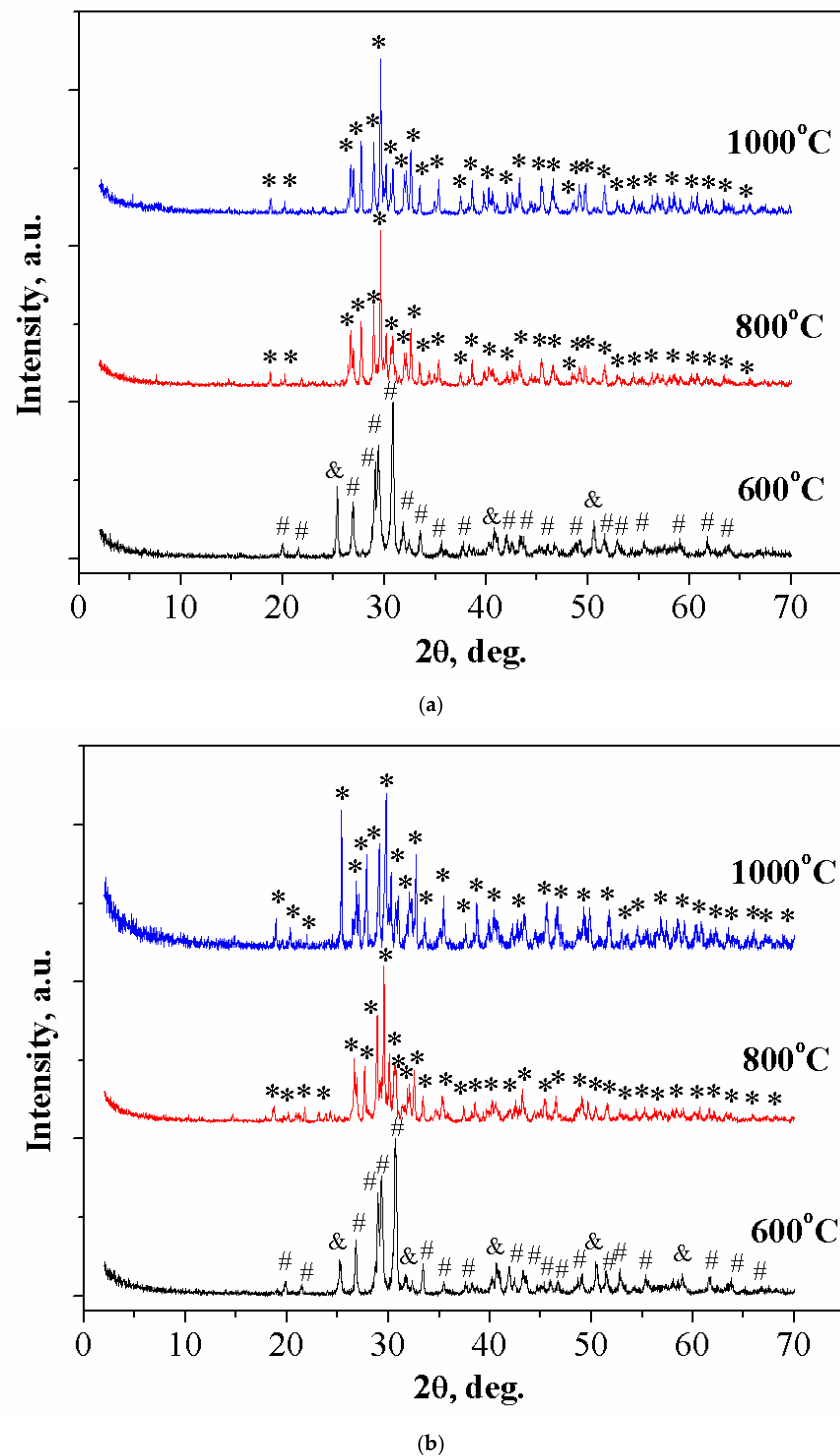
$$2Ca(PO_3)_2 + H_2O \rightarrow Ca_2P_2O_7 + 2HPO_3\uparrow \tag{15}$$

(**a**)

(**b**)
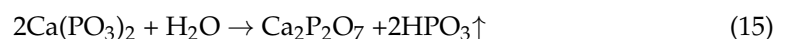
Figure 7. The XRD of ceramic materials with a weight ratio of: (**a**) $Ca(PO_3)_2/Ca_2P_2O_7 = 0/100$; *—$\beta$-$Ca_2P_2O_7$ (PDF 9-346); #—γ- $Ca_2P_2O_7$ (PDF 17-499); &—β-$Ca(PO_3)_2$ (PDF 17-500). (**b**) $Ca(PO_3)_2/Ca_2P_2O_7 = 20/80$ in the temperature range of 600–1000 °C.

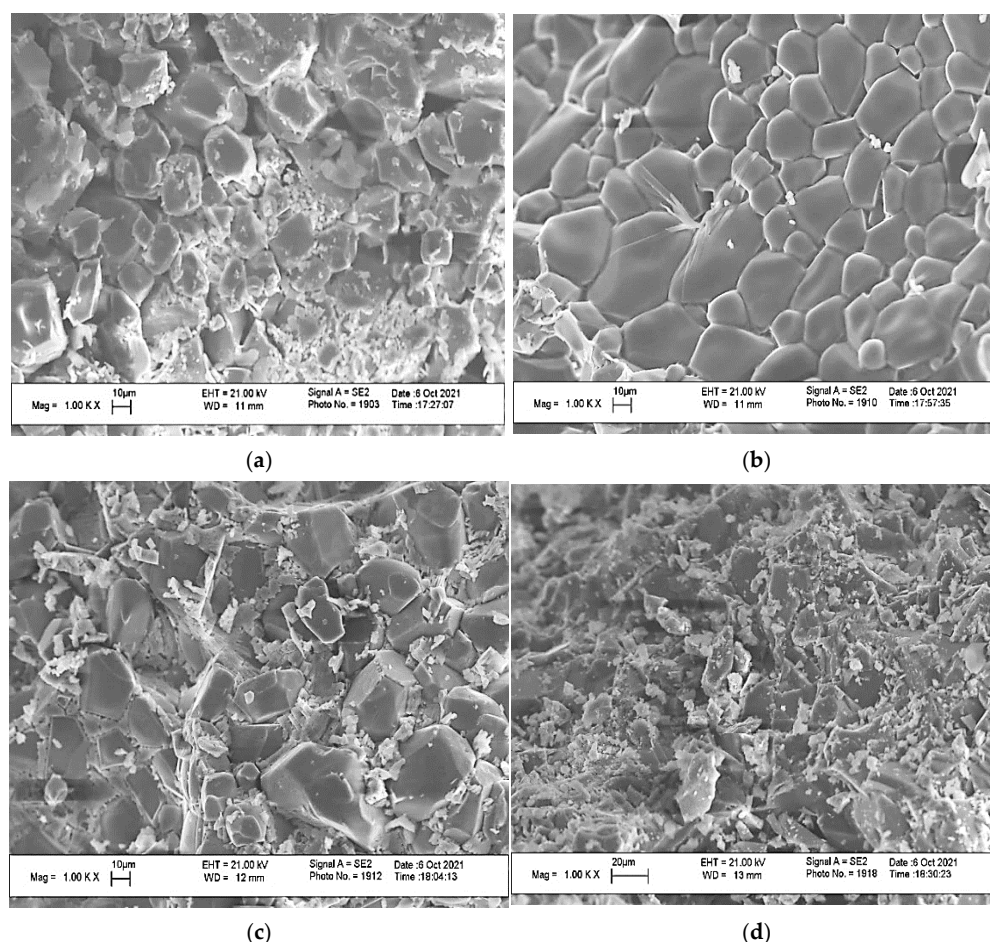The SEM images of the obtained samples after annealing at 1000 °C are shown in Figure 8.

Figure 8. The SEM images of the ceramic materials with a weight ratio of: (**a**) $Ca(PO_3)_2/Ca_2P_2O_7 = 0/100$; (**b**) $Ca(PO_3)_2/Ca_2P_2O_7 = 5/95$; (**c**) $Ca(PO_3)_2/Ca_2P_2O_7 = 10/90$; (**d**) $Ca(PO_3)_2/Ca_2P_2O_7 = 20/80$ at a temperature of 1000 °C.

The microstructure of the 0/100 ceramic material showed prismatic calcium pyrophosphate crystals of various sizes. The sample of ceramic material 5/95 displayed prismatic crystals of calcium pyrophosphate with smoothed edges, which was probably due to the melting above 950 °C of calcium polyphosphate formed by heating excess MCPM to temperatures above 500 °C. The decomposition of $Ca(PO_3)_2$, which initially formed a liquid phase, was observed in micrographs of compositions 10/95 and 20/80, where there were small crystals of calcium pyrophosphate crystallize in the intercrystalline space of calcium pyrophosphate. The 20/80 composition was distinguished by smaller crystals.

The relative density of the ceramic materials increased with an increase in the annealing temperature, reaching 43.7% at 1000 °C (Figure 9). For bulk samples, the increase in the relative density was negligible above 500 °C, which was associated with weight loss.

Figure 10 shows the temperature dependence of shrinkage for the ceramic materials.

Composition 20/80 presented the greatest shrinkage at all temperatures, gradually increasing from 600 to 1000 °C, while composition 10/90 showed a sharp increase in shrinkage to 1000 °C, which was probably associated with a large amount of liquid phase and recrystallization.

The strength of the ceramic matrices obtained by annealing a cement stone at 1000 °C exceeded several times the unannealed cement stone of compositions 20/80 and 10/90, while compositions 0/100 and 5/95 after annealing had lower strength characteristics than before annealing (Figure 11).
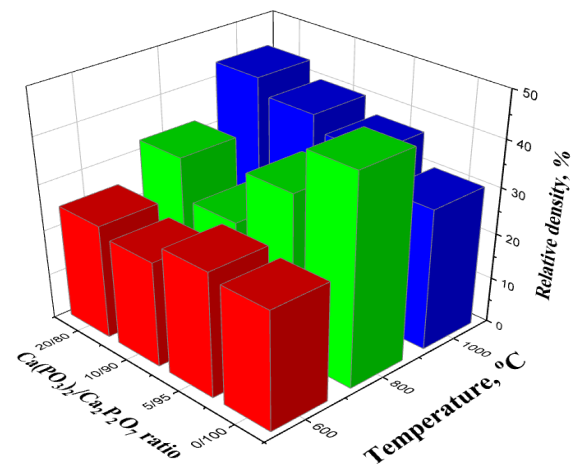
Figure 9. The relative density of samples with a weight ratio of: $Ca(PO_3)_2/Ca_2P_2O_7 = 0/100$; $Ca(PO_3)_2/Ca_2P_2O_7 = 5/95$; $Ca(PO_3)_2/Ca_2P_2O_7 = 10/90$; $Ca(PO_3)_2/Ca_2P_2O_7 = 20/80$ annealed in the temperature range of 600–1000 °C.
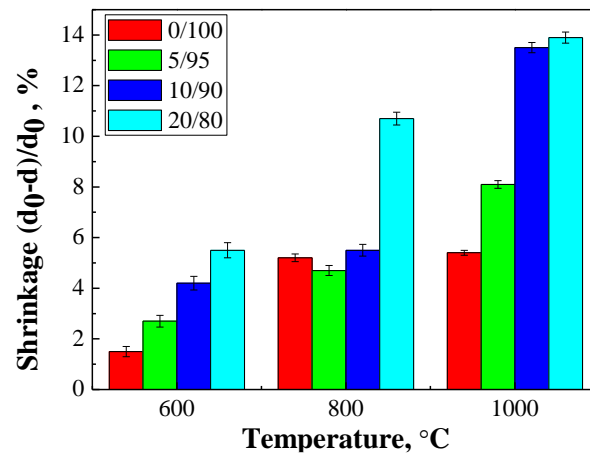
Figure 10. The shrinkage of the ceramic samples with a weight ratio of: $Ca(PO_3)_2/Ca_2P_2O_7 = 0/100$; $Ca(PO_3)_2/Ca_2P_2O_7 = 5/95$; $Ca(PO_3)_2/Ca_2P_2O_7 = 10/90$; $Ca(PO_3)_2/Ca_2P_2O_7 = 20/80$ in the range of 600–1000 °C temperatures.

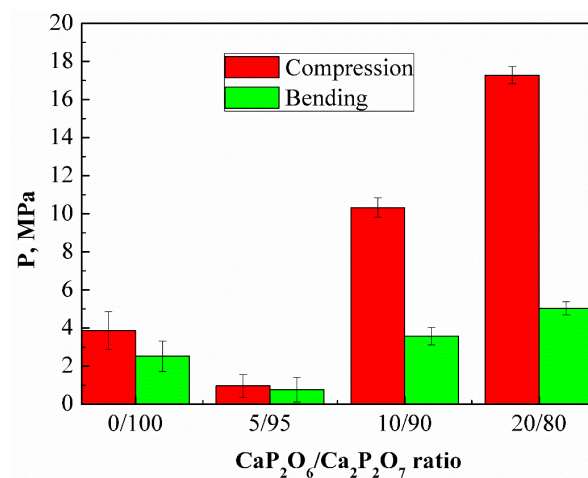**Figure 11.** The compressive and bending strengths of the samples with a weight ratio of: $Ca(PO_3)_2/Ca_2P_2O_7 = 0/100$; $Ca(PO_3)_2/Ca_2P_2O_7 = 5/95$; $Ca(PO_3)_2/Ca_2P_2O_7 = 10/90$; $Ca(PO_3)_2/Ca_2P_2O_7 = 20/80$ after annealing at a temperature of 1000 °C.

It is likely that an increase in the amount of polyphosphate due to excess MCPM in the initial mixture leads to liquid-phase sintering, improving the sintering ability and homogeneity of the ceramics, leading to an increase in the mechanical strength.

The true density of the cement stone decreases in all series from 0/100 to 20/80 (Figure 12), which was associated with the presence of MCPM in the initial composition.
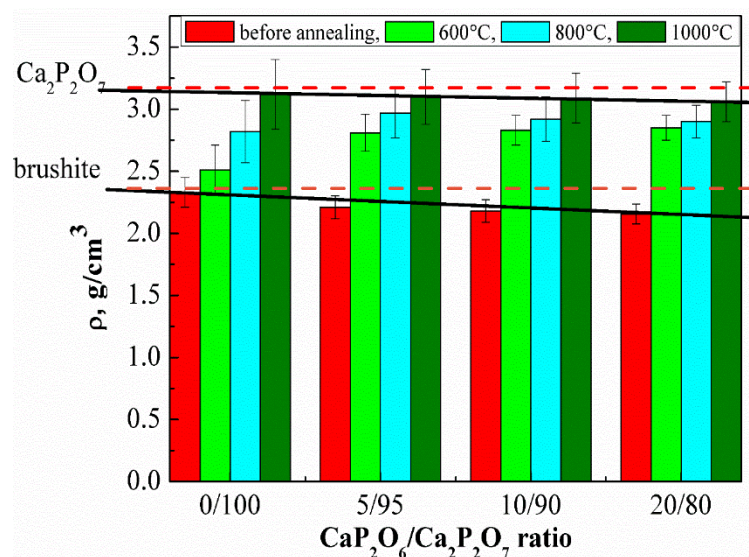

Figure 12. The true density of the ceramic materials before and after annealing in the temperature range of 600–1000 °C.

Dashed lines on the graph show the value of the true density for brushite ($\rho = 2.33$ g/cm^3) [29]. Solid lines show the values from our experiments. As seen in Figure 6, increasing the annealing temperature led to an increase in the true density of cement stone, which was associated with the recrystallization and formation of calcium pyrophosphate and polyphosphate. According to the literature, the true density of calcium pyrophosphate and calcium polyphosphate is 3.09 and 2.82 g/cm^3, respectively [30,31]. A more intense increase in the true density under the influence of temperature is characteristic for the compositions with a high MCPM content due to the formation of a lower-melting phase of calcium polyphosphate, which intensifies the sintering process.

When studying the behavior of porous ceramic materials in a solution that simulates the composition of interstitial fluid after 1 and 7 days, the formation of a characteristic open-work layer of apatite was observed, as can be seen from the SEM images (Figure 13). The results of the SBF sedimentation studies confirm that porous ceramic materials contribute to the crystallization of apatite from supersaturated solutions—analogues of interstitial fluids.

According to the results of the pH measurements of the aqueous solutions of the samples, the pure phase of calcium pyrophosphate (CaP$_2$O$_6$/Ca$_2$P$_2$O$_7$ = 0/100) had a virtually neutral pH level (Figure 14). As the calcium polyphosphate phase content increased, a slight acidification of the solution in the samples occurred. pH measurements of the obtained materials were conducted using aqueous solutions with a pH of 6.8, which is in the natural pH (6.4–8.4) range of the human body. Thus, the pH of the resulting materials is acceptable to the human body. Figure 15 shows the in vivo test results of the ceramic samples based on β–Ca$_2$P$_2$O$_7$, which annealed at 1000 °C.
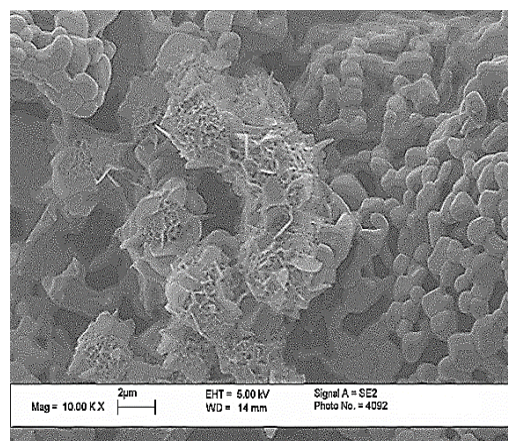
(**a**)
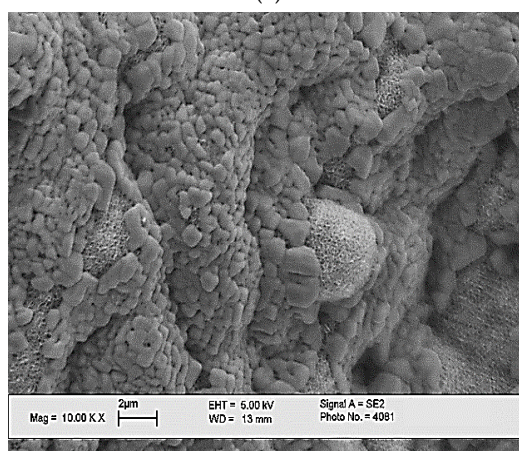
(**b**)

Figure 13. The SEM images of the surface of the ceramic sample with weight ratio of $Ca(PO_3)_2/Ca_2P_2O_7 = 0/100$ after mineralization for 1 day (**a**), and for 7 days (**b**) of the model medium SBF.
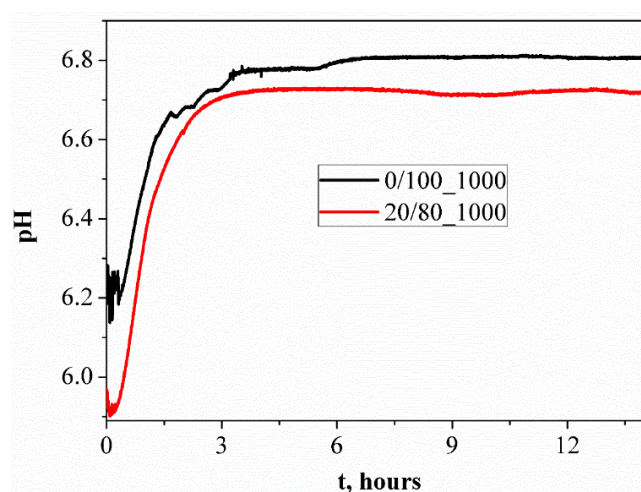

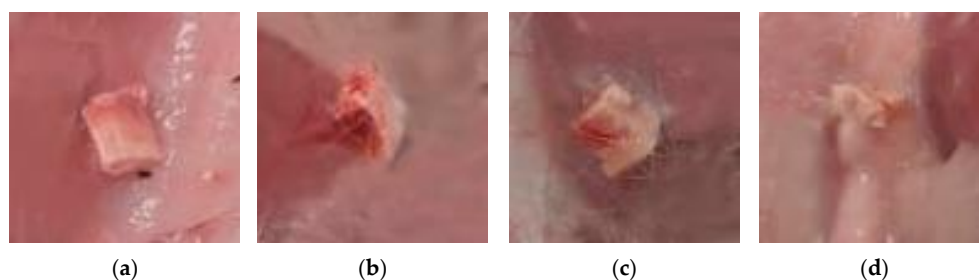**Figure 14.** The pH metering of the aqueous solutions of ceramic samples fired at 1000 °C.

Figure 15. Images of the ceramic materials with a weight ratio of: (a) $Ca(PO_3)_2/Ca_2P_2O_7 = 0/100$; (b) $Ca(PO_3)_2/Ca_2P_2O_7 = 5/95$; (c) $Ca(PO_3)_2/Ca_2P_2O_7 = 10/90$; (d) $Ca(PO_3)_2/Ca_2P_2O_7 = 20/80$ at a temperature of 1000 °C after implantation.

The best results of biocompatibility were possessed by the implants consisting of calcium pyrophosphate/calcium polyphosphate in ratios of 20/80 and 10/90 (Table 2).

Table 2. The in vivo test results.

Name of the Sample	0/100_1000	5/95_1000	10/90_1000	20/80_1000
Thickness capsule	3	3	3	4
Vascularization	2	2	1	1
Capsule maturity	1	3	4	4
Fibroblasts	1	1	3	3
Macrophages	0	2	3	3
Lympho-macrophage infiltration	0	2	3	4
Total	7	13	17	19

In these prototypes, thin, mature capsules formed with densely spaced and parallel oriented collagen fibers and few fibroblasts between them, with minimal inflammatory infiltration and vascularization. Less mature capsules formed around the implants of a different composition, in which the macrophage lining in the inner layer was partially retained and moderate lympho-macrophage infiltration and vascularization were noted.

4. Conclusions

Ceramic materials in $Ca_2P_2O_7$-$Ca(PO_3)_2$ system were obtained by annealing cement-salt stone based on powder mixtures of calcium citrate tetrahydrate $Ca_3(C_6H_5O_7)_2\cdot4H_2O$ and monocalcium phosphate monohydrate (MCPM) $Ca(H_2PO_4)_2\cdot H_2O$. These salts were mixed with each other in a such proportions that calcium pyrophosphate and calcium polyphosphate were in the final ceramic product in the following ratios: $Ca(PO_3)_2/Ca_2P_2O_7$ = 0/100; 5/95; 10/90 and 20/80. A lower melting phase of $Ca(PO_3)_2$ forming from an excess of $Ca(H_2PO_4)_2\cdot H_2O$ makes it possible to reduce the annealing temperature of ceramics.

The plastic strength of highly concentrated suspensions based on monocalcium phosphate monohydrate and calcium citrate tetrahydrate depends on the composition and hardening process, due to the formation of brushite/monetite phases. The increasing of plastic strength is associated with the process of hardening of cement solutions and formation of cement stone.

The use of calcium citrate tetrahydrate can significantly reduce the rate of formation of brushite, which makes it possible to use highly concentrated suspensions for extrusion 3D printing. Highly concentrated suspensions set and harden with the formation of cement stone, maintaining the shape of the matrix. Annealing of cement stone is accompanied by the following processes: the formation of the calcium pyrophosphate phase as a result of thermal transformation of calcium hydrophosphates; the conversion of unreacted chemical

binding of calcium citrate to calcium carbonate, and MCPM to calcium polyphosphate; the formation of the calcium pyrophosphate phase as a result of a heterophasic reaction of calcium carbonate and calcium polyphosphate.

In vivo tests of the obtained materials based on β—$Ca_2P_2O_7$ suggest that they can be recommended for regenerative treatments for bone defects.

Author Contributions: Conceptualization, O.T., T.S. (Tatiana Safronova), and M.K.; Methodology, T.S. (Tatiana Safronova); Investigation, O.T., T.S. (Tatiana Safronova), T.S. (Tatiana Shatalova), Y.L., E.K., and K.M.; Resources, S.S.; Visualization, O.T. and T.S. (Tatiana Shatalova); Writing—original draft, O.T. and T.S. (Tatiana Safronova); Writing—review & editing, O.T.; Supervision, T.S. (Tatiana Safronova); Project administration, T.S. (Tatiana Safronova). All authors have read and agreed to the published version of the manuscript.

Institutional Review Board Statement: The animal study protocol was approved by the Institutional Review Board (or Ethics Committee) of National Medical Research Center for Traumatology and Orthopedics named after N.N. Priorov, Ministry of Health of the Russian Federation (protocol code 005, date of approval 12.05.2021).

Informed Consent Statement: Not applicable.

Data Availability Statement: Not applicable.

Conflicts of Interest: The authors declare that they have no known competing financial interests or personal relationships that could have appeared to influence the work reported in this paper.

References

1.   Kucko, N.W.; Herber, R.-P.; Leeuwenburgh, S.C.G.; Jansen, J.A. Calcium Phosphate Bioceramics and Cements. *Princ. Regen. Med.* **2019**, *3*, 591–611.

2.   Salimi, E. Functionally graded calcium phosphate bioceramics: An overview of preparation and properties. *Ceram. Int.* **2020**, *46*, 19664–19668. [CrossRef]

3.   Safronova, T.V. Inorganic Materials for Regenerative Medicine. *Inorg. Mater.* **2021**, *57*, 443–474. [CrossRef]

4.   Safronova, T.V.; Kurbatova, S.A.; Shatalova, T.B.; Knotko, A.V.; Yevdokimov, P.V.; Putlyayev, V.I. Calcium pyrophosphate powder for production of bioceramics synthesized from pyrophosphoric acid and calcium acetate. *Inorg. Mater. Appl. Res.* **2017**, *8*, 118–125. [CrossRef]

5.   Safronova, T.V.; Shatalova, T.B.; Filippov, Y.Y.; Krut'ko, V.K.; Musskaya, O.N.; Safronov, A.S.; Toshev, O.U. Ceramics in the $Ca_2P_2O_7$–$Ca(PO_3)_2$ system obtained by annealing of the samples made from hardening mixtures based on calcium citrate tetrahydrate and monocalcium phosphate monohydrate. *Inorg. Mater. Appl. Res.* **2020**, *11*, 777–786. [CrossRef]

6.   Metsger, D.S.; Driskell, T.D.; Paulsrud, J.R. Tricalcium phosphate ceramic—A resorbable bone implant: Review and current status. *J. Am. Dent. Assoc.* **1982**, *105*, 1035–1038. [CrossRef]

7.   Daculsi, G. Biphasic calcium phosphate concept applied to artificial bone, implant coating and injectable bone substitute. *Biomaterials* **1998**, *19*, 1473–1478. [CrossRef]

8.   Valletregi, M. Calcium phosphates as substitution of bone tissues. *Prog. Solid State Chem.* **2004**, *32*, 1–31. [CrossRef]

9.   Habraken, W.; Habibovic, P.; Epple, M.; Bohner, M. Calcium phosphates in biomedical applications: Materials for the future? *Mater. Today* **2016**, *19*, 69–87. [CrossRef]

10. Canillas, M.; Pena, P.; de Aza, A.H.; Rodriguez, M.A. Calcium phosphates for biomedical applications. *Bol. Soc. Esp. Ceram. Vidr.* **2017**, *56*, 91–112. [CrossRef]

11. Bouler, J.M.; Pilet, P.; Gauthier, O.; Verron, E. Biphasic calcium phosphate ceramics for bone reconstruction: A review of biological response. *Acta Biomater.* **2017**, *53*, 1–12. [CrossRef] [PubMed]

12. Jeong, J.; Kim, J.H.; Shim, J.H.; Hwang, N.S.; Heo, C.Y. Bioactive calcium phosphate materials and applications in bone regeneration. *Biomater. Res.* **2019**, *23*, 4. [CrossRef] [PubMed]

13. Safronova, T.V.; Putlyaev, V.I. Powder systems for calcium phosphate ceramics. *Inorg. Mater.* **2017**, *53*, 17–26. [CrossRef]

14. Hurle, K.; Oliveira, J.M.; Reis, R.L.; Pina, S.; Goetz-Neunhoeffer, F. Ion-doped Brushite Cements for Bone Regeneration. *Acta Biomater.* **2021**, *123*, 51–71. [CrossRef]

15. Boanini, E.; Silingardi, F.; Gazzano, M.; Bigi, A. Synthesis and Hydrolysis of Brushite (DCPD): The Role of Ionic Substitution. *Cryst. Growth Des.* **2021**, *21*, 1689–1697. [CrossRef]

16. Zhou, H.; Yang, L.; Gbureck, U.; Bhaduri, S.B.; Sikder, P. Monetite, an important calcium phosphate compound–Its synthesis, properties and applications in orthopedics. *Acta Biomater.* **2021**, *127*, 41–55. [CrossRef]
17. Motameni, A.; Alshemary, A.Z.; Evisa, Z. A review of synthesis methods, properties and use of monetite cements as filler for bone defects. *Ceram. Int.* **2021**, *47*, 13245–13256. [CrossRef]
18. Safronova, T.V.; Putlyaev, V.I.; Kurbatova, S.A.; Shatalova, T.B.; Larionov, D.S.; Kozlov, D.A.; Evdokimov, P.V. Properties of amorphous calcium pyrophosphate powder synthesized via ion exchange for the preparation of bioceramics. *Inorg. Mater.* **2015**, *51*, 1177–1184. [CrossRef]
19. Lee, J.H.; Chang, B.-S.; Jeung, U.-O.; Park, K.-W.; Kim, M.-S.; Lee, C.-K. The first clinical trial of beta-calcium pyrophosphate as a novel bone graft extender in instrumented posterolateral lumbar fusion. *Clin. Orthop. Surg.* **2011**, *3*, 238. [CrossRef] [PubMed]
20. Safronova, T.V.; Putlyaev, V.I.; Ivanov, V.K.; Knot'ko, A.V.; Shatalova, T.B. Powders mixtures based on ammonium hydrophosphate and calcium carbonate for preparation of biocompatible porous ceramic in the CaO–P_2O_5 system. *Refract. Ind. Ceram.* **2016**, *56*, 502–509. [CrossRef]
21. Safronova, T.V.; Putlayev, V.I.; Bessonov, K.A.; Ivanov, V.K. Ceramics based on calcium pyrophosphate nanopowders. *Proc. Appl. Ceram.* **2013**, *7*, 9–14. [CrossRef]
22. Lin, F.-H.; Liao, C.-J.; Chen, K.S.; Sun, J.-S.; Liu, H.-C. Degradation behaviour of a new bioceramic: $Ca_2P_2O_7$ with addition of $Na_4P_2O_7 \bullet 10H_2O$. *Biomaterials* **1997**, *18*, 915–921. [CrossRef]
23. Webb, N.C. The crystal structure of β-$Ca_2P_2O_7$. *Acta Cryst.* **1966**, *21*, 942–948. [CrossRef]
24. Weil, M.; Puchberger, M.; Schmedt auf der Günne, J.; Weber, J. Synthesis, crystal structure, and characterization (Vibrational and Solid-State31P MAS NMR Spectroscopy) of the high-temperature modification of calciumcatena-polyphosphate(V). *Chem. Mater.* **2007**, *19*, 5067–5073. [CrossRef]
25. Kondrashenko, E.V.; Kondrashenko, V.I.; Kudryavtseva, V.D.; Grebennikov, D.A.; Semak, A.V. *Opredeleniye Plasticheskoy Prochnosti Rastvornykh i Betonnykh Smesey*; Library of National Technical University, Kharkiv Polytechnic Institute: Kharkiv, Ukraine, 2012.
26. Mirtchi, A.A.; Lemaitre, J.; Terao, N. Calcium phosphate cements: Study of the beta-tricalcium phosphate—Monocalcium phosphate system. *Biomaterials* **1989**, *10*, 475–480.
27. Mansour, S.A.A. Thermal decomposition of calcium citrate tetrahydrate. *Thermochimica acta* **1994**, *233*, 243–256. [CrossRef]
28. Hill, W.L.; Hendricks, S.B.; Fox, E.J.; Cady, J.G. Acid pyro-and metaphosphates produced by thermal decomposition of monocalcium phosphate. *Industrial & Engineering Chemistry* **1947**, *39*, 1667–1672.
29. Hill, W.L.; Hendricks, S.B. Composition and properties of superphosphate: Calcium phosphate and calcium sulfate constituents as shown by chemical and x-Ray diffraction Analysis. *Ind. Eng. Chem.* **1936**, *28*, 440–447. [CrossRef]
30. Schrödter, K.; Bettermann, G.; Staffel, T.; Wahl, F.; Klein, T.; Hofmann, T. Phosphoric acid and phosphates. *Ullmann's Encycl. Ind. Chem.* **2008**, *26*, 679–724.
31. Rothammel, W.; Burzlaff, H.; Specht, R. Structure of calcium metaphosphate $Ca(PO_3)_2$. *Acta Crystallogr. Sect. C Cryst. Struct. Commun.* **1989**, *45*, 551–553. [CrossRef]